

Field-Effect Tuned Adsorption Dynamics of VSe₂ Nanosheets for Enhanced Hydrogen Evolution Reaction

Mengyu Yan,^{†,‡} Xuelei Pan,[†] Peiyao Wang,[§] Fei Chen,[†] Liang He,[†] Gengping Jiang,^{||,§} Junhui Wang,[†] Jefferson Z. Liu,[§] Xu Xu,^{*,†} Xiaobin Liao,[†] Jihui Yang,[‡] and Liqiang Mai^{*,†}

[†]State Key Laboratory of Advanced Technology for Materials Synthesis and Processing, Wuhan University of Technology, Wuhan 430070, China

[‡]Materials Science and Engineering Department, University of Washington, Seattle, Washington 98195-2120, United States

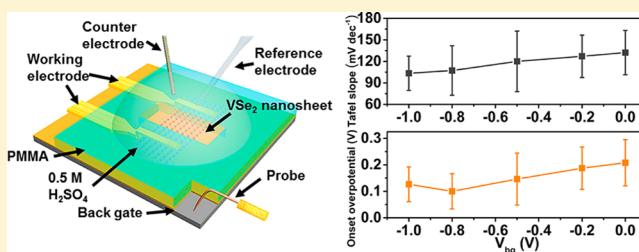
[§]Department of Mechanical and Aerospace Engineering, Monash University, Victoria 3800, Australia

^{||}College of Science, Wuhan University of Science and Technology, Wuhan 430081, China

S Supporting Information

ABSTRACT: Transition metal dichalcogenides, such as MoS₂ and VSe₂, have emerged as promising catalysts for the hydrogen evolution reaction (HER). Substantial work has been devoted to optimizing the catalytic performance by constructing materials with specific phases and morphologies. However, the optimization of adsorption/desorption process in HER is rare. Herein, we concentrate on tuning the dynamics of the adsorption process in HER by applying a back gate voltage to the pristine VSe₂ nanosheet. The back gate voltage induces the redistribution of the ions at the electrolyte–VSe₂ nanosheet interface, which realizes the enhanced electron transport process and facilitates the rate-limiting step (discharge process) under HER conditions. A considerable low onset overpotential of 70 mV is achieved in VSe₂ nanosheets without any chemical treatment. Such unexpected improvement is attributed to the field tuned adsorption-dynamics of VSe₂ nanosheet, which is demonstrated by the greatly optimized charge transfer resistance (from 1.03 to 0.15 MΩ) and time constant of the adsorption process (from 2.5 × 10⁻³ to 5.0 × 10⁻⁴ s). Our results demonstrate enhanced catalysis performance in the VSe₂ nanosheet by tuning the adsorption dynamics with a back gate, which provides new directions for improving the catalytic activity of non-noble materials.

KEYWORDS: Electrochemical catalysis, field effect, adsorption dynamics, hydrogen evolution reaction, VSe₂



Transition metal dichalcogenides (TMDCs) have been widely studied for decades, and recently two-dimensional layered thin TMDCs attract great interest in nanoelectronics,^{1,2} optoelectronics,^{3,4} and electrochemical energy storage^{5,6} aided by TMDCs' unique crystal and electronic band structure.^{6–8} Benefiting from the advancements above, electrochemical energy storage studies, focused on the electronic structure transformation to stimulate the conductivity of TMDCs, have achieved high-performance devices.^{9–12} Recent researches have suggested that an improved performance in hydrogen evolution reaction (HER) can be achieved via enhancing the conductivity of MoS₂ by phase transformation from the semiconducting 2H phase to the metallic 1T phase.^{9,10,13} However, these 1T products are thermodynamically unfavorable, and complicated chemical treatments are needed. A TMDC material with relatively high electrical conductivity would have the potential to promote the HER performance. Vanadium diselenide (VSe₂), which is a typical layered TMDC, has metallic properties and a high electrical conductivity ($G = \sim 1000$ S m⁻¹, at 300 K).^{14,15} VSe₂ has a CdI₂-type structure, where the V atom layer is sandwiched between two Se atom layers and the Se–V–Se layers are stacked by van der Waals interaction with

an interlayer spacing of 6.1 Å^{16,17} (Figure 1a). Recently, a one-pot colloidal route to obtain single-layer VSe₂ nanosheet has developed which shows an excellent HER performance with a low onset overpotential of 108 mV after oxygen plasma exposure.¹⁸

For an ideal HER process, besides the thermodynamic properties of catalysis, the dynamics of ions also plays a significant role.¹⁹ Different from the electronic structure which is intrinsic characteristics of different catalysts, the types of ions in the aqueous electrolyte are similar; thus, it is expected to design a more universal strategy to enhance the dynamics of ion transportation and optimize the overpotential. In the FET (field effect transistor) based electrochemical-liquid gate studies, it is found that the ion concentration in liquid can be controlled and the conductance of semiconductors can be altered by controlling the gate voltage.^{20,21} In light of these studies, the HER, a process influenced significantly by charge

Received: February 28, 2017

Revised: May 25, 2017

Published: June 6, 2017

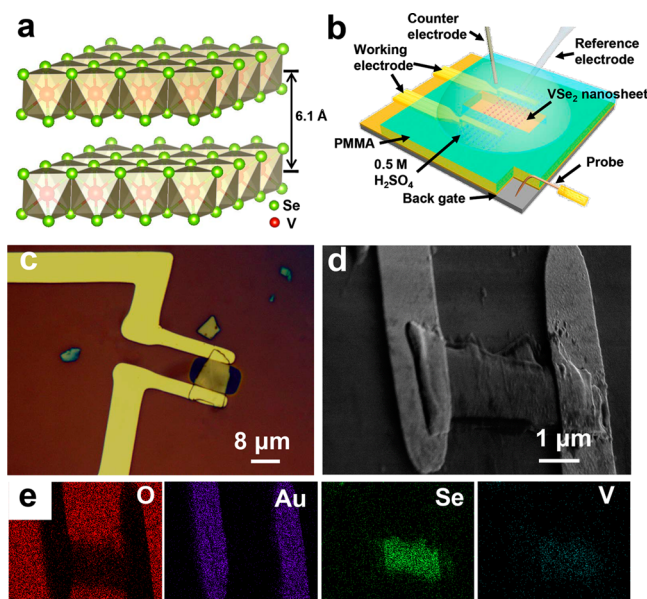


Figure 1. Morphology and working principle of the HER device. (a) Crystal structure model of VSe_2 . The interlayer spacing is 6.1 Å. The red balls represent V atoms, and the bright green balls represent Se atoms. (b) Schematic of the HER device. 0.5 M H_2SO_4 was used as the electrolyte. Heavily doped silicon (gray) is used as the back gate, and 300 nm SiO_2 (ocher) is used as the gate dielectric. Such devices enable easy control of different back gate voltages. (c) Optical micrograph of a typical VSe_2 nanosheet with two gold electrodes. (d) Scanning electron microscope (SEM) image and (e) corresponding elemental mapping of a typical VSe_2 nanosheet with two gold electrodes. The pattern of oxygen is to show the SiO_2 on the surface.

transfer rate and the dynamics of adsorption process, is also expected to be tuned by the field effect in theory.^{22,23}

Herein, we present a physical strategy to tune HER performance of the pristine VSe_2 nanosheet by applying a back gate voltage. This strategy achieves a decrease in the overpotential from 126 to 70 mV, which is almost comparable to the performance of Pt in our system. The result of electrochemical impedance spectroscopy (EIS) demonstrates that the R_{ct} decreases from 1.03 to 0.15 MΩ. Meanwhile, the high frequency time constant (τ_1) decreases from 2.5×10^{-3} to 5.0×10^{-4} s, which further proves the optimized adsorption process and facilitated discharge process (the rate-limiting step) during HER. Afterward, we confirmed our results by in situ I - V measurement. Along with the increase of overpotential, the resistance of VSe_2 greatly decreased due to the redistribution of ions in the electrolyte and charges on the VSe_2 nanosheet surface, which contributes to the decrease of R_{ct} .

In this work, a Scotch-tape based mechanical exfoliation method²⁴ was used to exfoliate the bulk VSe_2 (single crystal) to obtain VSe_2 flakes. The XRD patterns of bulk and as-exfoliated VSe_2 are shown in Figure S1. The high-resolution X-ray photoelectron spectroscopy (XPS) curves are shown in Figure S2. The peaks at 514.1 and 521.5 eV are assigned to V $2p_{3/2}$ and V $2p_{1/2}$, which indicate the V^{4+} oxidation state. The peaks located at 54.2 and 55.0 eV can be attributed to Se $2p_{5/2}$ and S $2p_{3/2}$, respectively. Subsequently, VSe_2 nanosheets were transferred to a prepatterned Si/ SiO_2 substrate. E-beam lithography (EBL) and physical vapor deposition (PVD) were performed to fabricate the gold electrodes which connect the individual VSe_2 nanosheet to outer contact pads. At last, poly(methyl methacrylate) (PMMA) was used as insulating

layer, and rectangular windows were opened using EBL (see details in Figure S3). The working principle and morphology of the electrochemical device are shown in Figure 1b and c. The atomic force microscopic image is shown in Figure S4, which indicates that the thickness of VSe_2 nanosheet is around 35 nm. I - V measurement results with PMMA insulating layer suggest that the leak current is ~ 1 pA which is negligible during the measurement with active materials (Figure S5a). In this way, this device is stable enough to provide precise measurement results. The SEM image of a specific device is presented in Figure 1d, and Figure 1e is the corresponding element mapping. It is demonstrated that our fabrication method ensures that gold electrodes are well-attached to the surface of SiO_2 and the individual VSe_2 nanosheet is well-bonded to gold electrodes.

On the basis of the fabricated devices, a standard three-electrode configuration was realized. A platinum wire electrode was used as the counter electrode, and a saturated calomel electrode (SCE) was used as the reference electrode. The polarization curves of Pt, VSe_2 , Au, and PMMA are shown in Figure 2a. The results show that the onset overpotential of Au

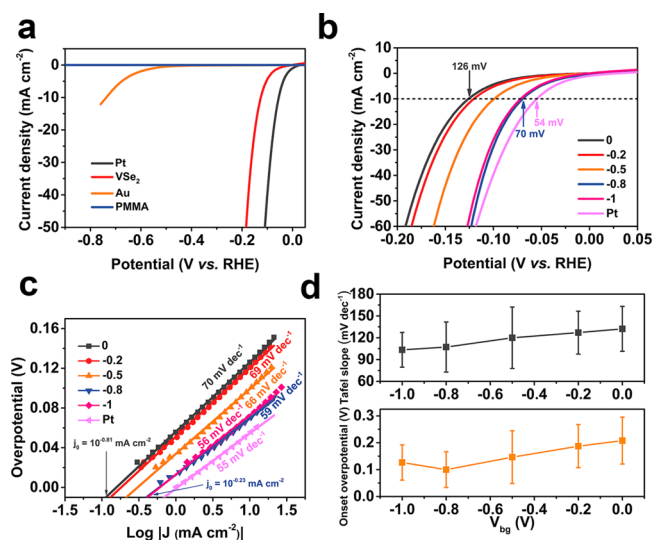


Figure 2. HER activity of individual VSe_2 nanosheet. (a) Polarization curves of PMMA, Au, VSe_2 and Pt. (b) Polarization curves of VSe_2 measured at different back gate voltages ($V_{\text{bg}} = 0, -0.2, -0.5, -0.8,$ and -1.0 V). (c) Corresponding Tafel plot of an individual VSe_2 nanosheet. (d) Statistic-based influence of the back gate on the onset overpotential and Tafel slope. The square dots are the average values, and the error bar represents standard error.

is ~ 500 mV and PMMA does not show obvious HER activity, which indicates that the PMMA insulating layer is suitable for this electrochemical measurement. Also, the pristine VSe_2 shows effective catalytic performance. The polarization curve of VSe_2 in Figure 2a reflects the optimal performance of the pristine VSe_2 nanosheets, which has an onset overpotential of 126 mV at a current density of 10 mA cm^{-2} and Tafel slope of 70 mV dec^{-1} (see calculation methods in Supporting Information). To make better comparison, the HER performance of sputtered micro-sized Pt working electrode is set as the control sample (see more details in Figure S7). The onset overpotential of Pt is 54 mV at a current density of 10 mA cm^{-2} , and the Tafel slope is 55 mV dec^{-1} .

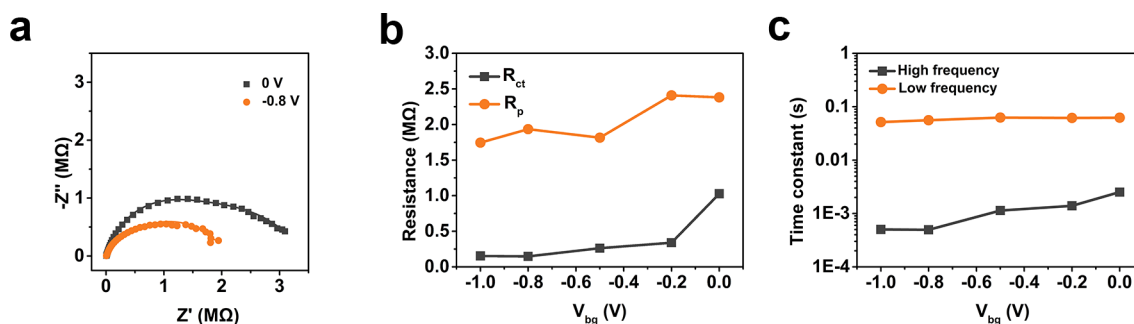
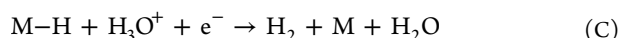
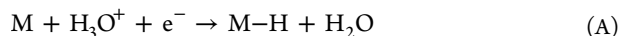


Figure 3. Electrochemical impedance spectroscopy and kinetic analysis. (a) Nyquist plots of individual VSe₂ nanosheet at different back gate voltage ($V_{bg} = 0$ V and -0.8 V). The set potential is -0.4 V vs RHE. The dots and lines are the experiment and fitting data, respectively. (b) Plot of R_{ct} and R_p . (c) Plot of a corresponding high-frequency time constant (τ_1) and low-frequency time constant (τ_2).

It is generally acknowledged that there exist two mechanisms for HER in acid solution, termed as the Volmer–Tafel mechanism (reaction A and B) and the Volmer–Heyrovsky mechanism (reactions A and C),^{25–27}



where M represents the electrode material and M–H represents the hydrogen adsorbed on the electrode surface. According to the Butler–Volmer equation, the Tafel slope can be used to determine the reaction mechanism.²⁸ For most VSe₂ nanosheets, the Tafel slopes are higher than 116 mV dec^{-1} (4.6 RT/F) or around it, which is thought to be a factor for judging whether the discharge process (step A) is the rate-limiting step.²⁹ In detail, step A (discharge process/Volmer reaction) involves two parts: the hydroxonium ion (H_3O^+) diffuses to the surface of the electrode, and then H_3O^+ picks up an electron and generates hydrogen adsorbed on the electrode surface.^{30,31} To enhance the reaction rate and corresponding catalytic performance, we should concentrate on enhancing the concentration of available H_3O^+ . Inspired by the former researches on FETs,^{1,32,33} we try to apply the back gate voltage in the electrochemical devices to tune the HER performance of individual VSe₂ nanosheet by facilitating the concentration of H_3O^+ .³⁴ The back gate was realized by a probe connected to the Si substrate where the SiO₂ was thoroughly removed. The polarization curves measured at different back gate voltages (V_{bg}) are shown in Figure 2b. It is obvious that HER performance improves along with the increase of the negative back gate voltage. The onset overpotential is optimized from 126 to 70 mV (at a current density of 10 mA cm^{-2}), and the Tafel slope decreases from 70 to 59 mV dec^{-1} (Figure 2c) which is almost comparable to the performance of Pt in our system. Although this merely reveals the best performance, the change rule is obvious and important. Also, the exchange current density j_0 increases from $10^{-0.81}$ to $10^{-0.23} \text{ mA cm}^{-2}$, which reveals the enhanced catalytic ability at equilibrium. It may attribute to that the back gate voltage induced the redistribution of the ions in the electrolyte; thus the H_3O^+ ions concentrate on the surface of the VSe₂ nanosheet, which facilitates the discharge process.³⁰ Meanwhile, a limitation of the optimization is also observed. When V_{bg} reaches -1 V, the HER performance is no longer optimized but goes bad to some extent. To uncover a statistical change trend, dozens of VSe₂ nanosheets based HER devices were tested under a different

back gate voltage (Figure 2d). The average onset overpotential and Tafel slope display an obvious decreasing trend with the decrease of the back gate voltage, which further proves that the back gate induced improvement of HER performance is a real effect. An obvious slower change appears at $V_{bg} = -1$ V, which confirms the conclusion aforementioned. Traditional electrode materials are difficult to precisely calculate the turnover frequency (TOF) value because of the difficulty in quantifying the density of activity sites.^{35,36} Meanwhile, thanks to the individual VSe₂ nanosheet device, we can easily calculate the area of the electrode and achieve a precise estimated active sites number.^{11,37} In this work, applying a back gate voltage is a physical strategy which is not able to change the density of active sites. Thus, the TOF value can be calculated with a constant density of active sites. It is found that the TOF value increases with the back gate voltage (Figure S9). Meanwhile, considering the similar configuration for the measurement and the calculation methods, the TOF values are comparable to the data of MoS₂ in ref 11. The variation of TOF value is contributed from the increased reaction rate and activity of per sites on condition that a constant density of active sites does not contribute to the increasing current density, which results in an accelerated dynamics process of HER.

For further investigation of influence from the back gate, electrochemical impedance spectroscopy (EIS) was applied to investigate the electrode kinetics under HER condition.^{26,38} The Nyquist plots from different gate voltages are shown in Figure 3a and Figure S10. (See more details of fitting and calculation in Supporting Information.) The Nyquist plots indicate a two-time constant model as two linked semicircles appears on the complex plane without a diffusion control. The impedance spectra of different back gate voltages were fitted to a modified Armstrong's equivalent circuit (Figure S10a inset). The plot of charge transfer resistance (R_{ct}) and electro-desorption or recombination reaction resistance (R_p) is shown in Figure 3b. With the V_{bg} decreases from 0 V to -1 V, the corresponding R_{ct} dramatically drops from 1.03 to 0.15 MΩ and R_p falls from 2.38 to 1.78 MΩ. The high frequency time constant, τ_1 also goes through a dramatic decrease (from 2.5×10^{-3} to 5.0×10^{-4} s) (Figure 3c), and the low frequency time constant, τ_2 almost remains unchanged. The corresponding percentage change plots are shown in Figure S10f. Also, the change trend is consistent with the rule of optimization. It is obvious that the high-frequency region does changed a lot when applied back gate voltage. According to theory of Armstrong,^{39,40} time constant (τ) measures the rate of that θ relaxes to new value at a changed potential. R_{ct} represents the

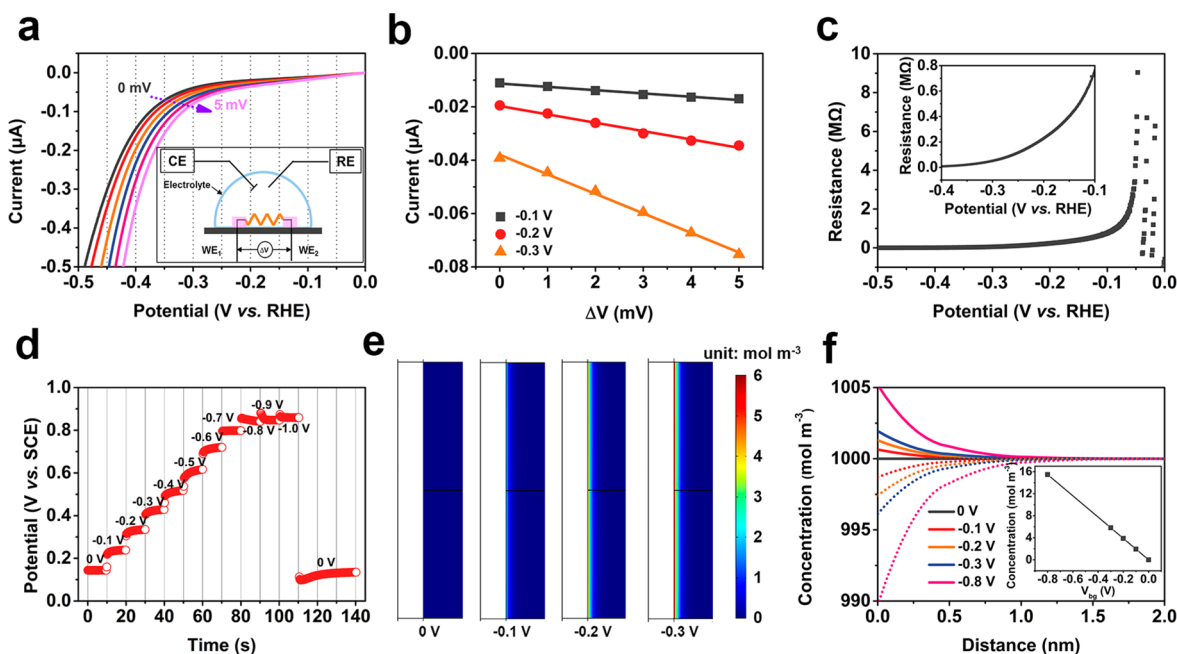


Figure 4. In situ I – V measurement under HER condition and gate-dependent potential and current. (a) Polarization curves from different ΔV ($\Delta V = V_1 - V_2$, where V_1 and V_2 represent potential applied on the working electrode 1 and 2). Inset: The schematic of the circuit for the in situ I – V measurement. CE, counter electrode; RE, reference electrode; WE, working electrode. (b) The linear relationship between ΔV and the current (including catalytic and materials induced current) when the potential is -0.1 , -0.2 , and -0.3 V, respectively. The dots are experimental data, and the lines are the fitting data. (c) Plot of resistance of VSe_2 nanosheet during the potential linear sweep process. Inset: the partial curves (from -0.1 V to -0.4 V). (d) Gate-dependent open circuit potential (vs SCE) of VSe_2 nanosheet in 0.5 M H_2SO_4 . Each step is -0.1 V, and it holds for 10 s. (e) Stationary state of net charge concentration distribution in electrolyte region under different additional potential biases induced (0 , -0.1 , -0.2 , -0.3 V). (f) Concentration of positive and negative charges (line represents H^+ , and dots represent SO_4^{2-} , respectively) and the net charge (inset) under different additional potential biases induced (0 , -0.1 , -0.2 , -0.3 , -0.8 V).

equivalent Faradaic resistance for charge transfer resistance. The reduction of these two parameters demonstrate the faster rate and smaller obstacle for interfacial electrochemical reaction. When V_{bg} reaches -1 V, R_{ct} and τ_1 will not change any more and even increase a little. According to the two-time constant model, the high-frequency region represents the charge transfer process, and these results suggest that the back gate mainly acts on the charge transfer reaction.^{37,41} When the negative back gate electric field is applied on the nanosheet, H_3O^+ ions concentrate on the outer surface of nanosheet, and the charge carriers concentrate on the inner surface, which facilitates the electron transport and the charge transfer reaction.²¹ These results confirm the change tendency of HER performance under different back gate voltages. Gupta et al. have come to a similar conclusion through the gate-dependent electrochemical HER measurements.⁴² The conductivity of MoS_2 greatly increases with a back gate voltage, and consequently the HER performance is improved. However, under a dry condition (without electrolyte), the typical VSe_2 nanosheet does not show a semiconductor characteristic; the conductivity keeps constant with the change of the back gate voltage (Figure S11). Therefore, the electrical transport characteristic of the individual VSe_2 nanosheet in the electrolyte needs to be tested.

The electrical double layer model shows that the change of electrode potential will cause a change in the surface charge, which is attributed to a redistribution of the electrical double layer of charged ions and dipoles.⁴³ When the potential linear sweeps from 0 V to -0.5 V vs RHE, the surface ions and the current carriers will redistribute around the interface between electrolyte and catalyst. So the change of overpotential is also

supposed to change the electron transport properties. In order to investigate the changing process, a circuit is designed as shown in Figure 4a. In this circuit, an additional working electrode is added to measure the electrical transporting properties during the LSV process. Although these two working electrodes (applied different electrode potentials) belong to a three-electrode circuit, the electrical signals are recorded respectively for further calculation. In a typical measurement process, V_1 and V_2 reduced synchronously with a constant ΔV ($\Delta V = V_1 - V_2$) kept between them (the potential applied to WE_1 and WE_2 are assigned as V_1 and V_2 , respectively).⁴⁴ The differences between the two WEs attribute to ΔV , and the differences reflect the electrical transportation properties at a specific electrode potential. In this way, the Faradaic current contributed from HER reaction can be offset by subtracting the original current value ($\Delta V = 0$) from the current value ($\Delta V \neq 0$). Thus, the resistance value can be calculated from ΔV and ΔI . It is supposed that the little voltage difference (1 – 5 mV) between working electrodes will barely affect the measurement, because ΔV is much less than onset overpotential. The polarization curves from different ΔV , ranging from 0 to 5 mV, are shown in Figure 4a. Due to the reversibility of the distribution of ions, the resistance values at the same potential should be almost the same.³⁰ So the current values should be linear to ΔV . The measurement results confirm this speculation. An excellent linear relationship between current values and ΔV is obtained with the overpotential of -0.1 , -0.2 , and -0.3 V (Figure 4b). This linear relationship proves the accuracy of these calculated results, and the reciprocal of slope represents resistance. A decreasing tendency of resistance is observed from slopes of the three lines. For convenience, we

calculate the average resistance value from different ΔV (Figure 4c).

The in situ I - V result demonstrates that the resistance of electrode material (VSe₂ nanosheet) decreases with the decreasing potential. The adsorption of H atoms results in the decreasing resistance of the electrode material, and a similar result is observed in Pt nanowires.⁴⁴ The adsorbed H atoms change the electrical transport property, which surely acts on the electrochemical process. This interesting result is consistent with reported results on the liquid-gated FET³⁰ and the theory of Conway.⁴⁵ According to the equation of $\Delta H_\theta = \Delta H_0 - r\theta_H$, where r is a coefficient, ΔH_0 is the initial heat of adsorption, ΔH_θ is the heat of adsorption of H, and θ_H is the coverage of adsorbed H, it can be found that the θ_H is a function of potential, which is a linear dependence of θ_H on potential in a specific region, and ΔH_θ is assumed to be a linear function of θ_H . During the catalytic process, the change of overpotential induces the redistribution of ions, and the adsorption of H atoms contributes to the reduced barrier for charge transfer on the interface.

When back gate voltage is applied to the nanosheet, the ions will be redistributed, and the concentration gradient will form under a steady state. According to the Nernst equation, the concentration gradient is to change the output voltage of the cell. To measure the gate-dependent concentration gradient, the gate-dependent open circuit potential (V_{ocp}) is measured (Figure 4d). The potential difference between WE and RE is measured when the V_{bg} varies from 0 V to -1 V. When V_{bg} is lower than -0.8 V, V_{ocp} does not increase any more and nearly remains constant. This interesting result is consistent with the variation of gate-dependent HER performance in VSe₂ as well as the EIS results, which shows a limited optimization when V_{bg} is around -0.8 V. These results further confirm that the gate field directly acts on the accumulation of H⁺. When considering the saturation of V_{ocp} , we think it is mostly similar to the electrolyte starvation effect.^{46–48} Conway has demonstrated that the highly accumulated ions in dilute electrolyte will limit the increase of double layer capacity with the decreased conductivity of the electrolyte.⁴⁹ Although this system is not completely consistent with an electrochemical capacitor, the limitation of the accumulation of ions is also reasonable. The concentrated ions will reach a balance with the diffused ions. To confirm our theory, the gate-dependent HER performance of Au is measured in our devices. The HER performance shows a vivid optimization when negative V_{bg} is applied and the limit V_{bg} is around -1.2 V (Figure S8). It is obvious that this is consistent with the variation of V_{ocp} , which also shows saturated phenomenon. These results demonstrate that the gate induced accumulation of ions is responsible for the optimization of HER performance directly.

To identify the change rule of ion distribution at different back gate voltages, a continuum simulation method was utilized (Figure S12). Figure 4e is the stationary state of net charge concentration distribution in the electrolyte region with additional potential bias induced. Figure 4f is the corresponding H⁺ concentration along the middle line for different potential bias. It is obvious that the back gate voltage induces the redistribution of ions in the bulk electrolyte and increases H⁺ concentration on the surface of SiO₂. Despite this model is hardly to uncover the change in Helmholtz layer, the variation confirms the experiment results solidly. The concentration distributions of different initial concentrations (1, 10, and 100 mol m⁻³) are presented in Figure S13a–c. Additionally, a

percentage variation of different initial concentrations is shown in Figure S13d. This curve vividly shows an accelerated tendency of increasing ratio when H⁺ concentration is decreased, which proves a more efficient optimization at lower concentration of H⁺. It is noted that the net charge increased a lot compared to the origin state, which indicates more available protons and less SO₄²⁻.

On the basis of the results above, we can draw a conclusion that both the back gate voltage and the adding negative electrode potential on the nanosheets directly can result in the distribution of ions and increase the coverage of adsorbed H atoms.⁵⁰ Thus, the oriented distribution of ions on the electrolyte–electrode material interface is responsible for the improvement of HER performance, which results in the less heat of adsorption and faster charge transfer process. Liu et al. have reported the similar conclusion in the work about field-enhanced electrocatalytic CO₂ reduction,⁵¹ which shows that a field induced concentration of reagent boosts the catalytic reaction. In our work, the concentration of surface H₃O⁺ induces the increased coverage of H, causing the change of electron transport property as well as the barrier for charge transfer process. This further tunes the adsorption dynamics which is the fundamental reason for the enhanced HER performance.

To confirm the validity of the field induced concentration under a steady state, the chronoamperometry measurement at constant potential was performed (Figure 5a). The current

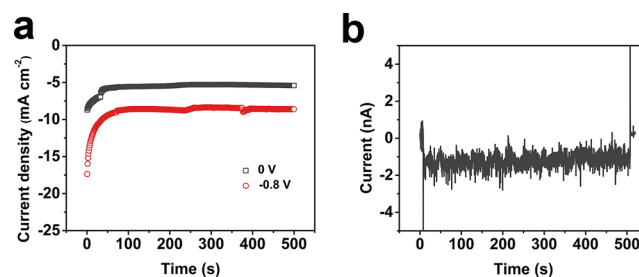


Figure 5. Chronoamperometry measurement. (a) Chronoamperometry measurement of VSe₂ at a constant applied potential of -0.4 V vs SCE ($V_{bg} = 0$ V and -0.8 V). (b) Time-dependent gate current ($V_{bg} = -0.8$ V) during the chronoamperometry measurement.

density increased a lot at the beginning of measurement; then the current density decreased to a steady region. Here, we did not measure data for a much longer time as the electrolyte is a droplet of H₂SO₄ solution, which cannot be afforded for long-time consumption. Also, the corresponding gate current is recorded to show the consumption of the gate (Figure 5b). The gate current is ~ 1.3 nA, which is much smaller than the increased current. If considering the area difference of gate and the nanosheet, the current density will show great advantages.

In this work, we present a new strategy to improve the HER performance through a physical method using the back gate to tune the distribution of ions in the electrolyte and on the surface of electrode material (VSe₂ nanosheet). The measurement results show an optimization of onset overpotential from 126 to 70 mV and a Tafel slope from 70 to 59 mV dec⁻¹. The R_{ct} decreases from 1.03 to 0.15 M Ω , and the high frequency time constant decreases from 2.5×10^{-3} to 5.0×10^{-4} s, suggesting that the back gate electric field facilitates the discharge process, the rate-limiting step for the HER of VSe₂

nanosheet. We believe these results will provide new directions for improving the catalytic activity of non-noble materials.

Experimental Section. *Fabrication of the Individual VSe₂ Nanosheet Electrochemical Device.* The bulk VSe₂ crystal (99.995%) was bought from Nanjing XFNANO Materials Tech Co., Ltd. The multilayered VSe₂ nanosheets were obtained by Scotch-tape based mechanical exfoliation of the bulk VSe₂ sample and subsequently transferred onto the Si/SiO₂ substrate which has patterned outer contact pads through a conventional photolithography process. Afterward, the inner microelectrodes (Cr/Au, 5/150 nm) were fabricated by EBL and thermal evaporation deposition. At last, open windows by EBL after spin-coating PMMA.

Material and Device Characterization. The SEM images and element mapping of the fabricated devices were recorded using a JEOL JSM-7001F microscope at an acceleration voltage of 20 kV and an energy-dispersive spectroscopy system (INCA X/MAX 250). XRD (Burker D8 Advanced X-ray diffractometer with Cu-K α radiation) was employed to characterize the structural phases of the samples. XPS (ESCALAB 250Xi, Thermo Scientific) was used to analyze the composition of samples with Al K α radiation. The Autolab 302N, probe station (Lake Shore, TTPX), and semiconductor device analyzer (Agilent B1500A) were used to measure the electrochemical performance of the device. The atomic force microscopy image was obtained using scanning probe microscopy (Bruker MultiMode VIII).

Electrochemical Measurement. In this three-electrode configuration, platinum wire electrode and saturated calomel electrode (SCE) worked as the counter electrode and the reference electrode, respectively. 0.5 M H₂SO₄ was used as the electrolyte. The probe station combined with semiconductor device analyzer were used to measure the electrical transport characteristics of the individual nanosheet. The HER performance of VSe₂ nanosheet under different gate voltages was tested by combining electrochemical workstation with the probe station and semiconductor device analyzer. The polarization curve of HER was measured by linear sweep voltammetry at a scan rate of 5 mV s⁻¹.

In Situ I–V Measurement. In this section, the probe station and semiconductor device analyzer are used to realize the in situ I–V measurement. Four standard source–measure unit (SMU) channels are connected to two working electrodes, the counter electrode and the reference electrode, respectively. The two SMU channels connected to WE₁ and WE₂ are used to supply potential to perform a typical linear sweep voltammetry measurement with a constant difference of potential between them (ranging from 0 to 5 mV).

■ ASSOCIATED CONTENT

Supporting Information

The Supporting Information is available free of charge on the ACS Publications website at DOI: 10.1021/acs.nanolett.7b00855.

Additional information and figures (PDF)

■ AUTHOR INFORMATION

Corresponding Authors

*E-mail: mlq518@whut.edu.cn.

*E-mail: xuxu@whut.edu.cn.

ORCID

Jefferson Z. Liu: 0000-0002-5282-7945

Liqiang Mai: 0000-0003-4259-7725

Author Contributions

M.Y.Y. and X.L.P. contributed equally to this work. L.Q.M., M.Y.Y., and F.C. designed the experiments. X.L.P., M.Y.Y., P.Y.W., and J.H.W. performed the experiments. P.Y.W., G.P.J., and J.Z.L. carried out the COMSOL simulation. M.Y.Y., X.L.P., J.H.W., X.X., X.B.L., L.H., J.H.Y., G.P.J., and J.Z.L. discussed the interpretation of results and cowrote the paper. All authors discussed the results and commented on the manuscript.

Notes

The authors declare no competing financial interest.

■ ACKNOWLEDGMENTS

This work was supported by the National Key Research and Development Program of China (No. 2016YFA0202603 and 2016YFA0202604), the National Basic Research Program of China (2013CB934103), the Programme of Introducing Talents of Discipline to Universities (B17034), the National Natural Science Foundation of China (51521001), the National Natural Science Fund for Distinguished Young Scholars (51425204), the China Postdoctoral Science Foundation (No. 2015T80845), the Fundamental Research Funds for the Central Universities (WUT: 2016III001, 2016III005) and the National Students Innovation and Entrepreneurship Training Program (WUT: 20161049701003). M.Y. Yan would like to acknowledge the support from the State of Washington through the University of Washington Clean Energy Institute.

■ REFERENCES

- Radisavljevic, B.; Radenovic, A.; Brivio, J.; Giacometti, V.; Kis, A. *Nat. Nanotechnol.* **2011**, *6*, 147–50.
- Zhu, C.; Zeng, Z.; Li, H.; Li, F.; Fan, C.; Zhang, H. *J. Am. Chem. Soc.* **2013**, *135*, 5998–6001.
- Yin, Z.; Li, H.; Li, H.; Jiang, L.; Shi, Y.; Sun, Y.; Lu, G.; Zhang, Q.; Chen, X.; Zhang, H. *ACS Nano* **2012**, *6*, 74–80.
- Choi, M. S.; Qu, D.; Lee, D.; Liu, X.; Watanabe, K.; Taniguchi, T.; Yoo, W. J. *ACS Nano* **2014**, *8*, 9332–9340.
- Xiong, F.; Wang, H.; Liu, X.; Sun, J.; Brongersma, M.; Pop, E.; Cui, Y. *Nano Lett.* **2015**, *15*, 6777–84.
- Jiang, H.; Ren, D.; Wang, H.; Hu, Y.; Guo, S.; Yuan, H.; Hu, P.; Zhang, L.; Li, C. *Adv. Mater.* **2015**, *27*, 3687–3695.
- Wang, Q. H.; Kalantar-Zadeh, K.; Kis, A.; Coleman, J. N.; Strano, M. S. *Nat. Nanotechnol.* **2012**, *7*, 699–712.
- Chhowalla, M.; Shin, H. S.; Eda, G.; Li, L.-J.; Loh, K. P.; Zhang, H. *Nat. Chem.* **2013**, *5*, 263–275.
- Acerce, M.; Voiry, D.; Chhowalla, M. *Nat. Nanotechnol.* **2015**, *10*, 313–8.
- Lin, Y.-C.; Dumcenco, D. O.; Huang, Y.-S.; Suenaga, K. *Nat. Nanotechnol.* **2014**, *9*, 391–396.
- Voiry, D.; Yang, J.; Chhowalla, M. *Adv. Mater.* **2016**, *28*, 6197–206.
- Cai, P.; Huang, J.; Chen, J.; Wen, Z. *Angew. Chem., Int. Ed.* **2017**, *56*, 4858–4861.
- Lukowski, M. A.; Daniel, A. S.; Meng, F.; Forticaux, A.; Li, L.; Jin, S. *J. Am. Chem. Soc.* **2013**, *135*, 10274–7.
- Xu, K.; Chen, P.; Li, X.; Wu, C.; Guo, Y.; Zhao, J.; Wu, X.; Xie, Y. *Angew. Chem., Int. Ed.* **2013**, *52*, 10477–81.
- Woolley, A. M.; Wexler, G. *J. Phys. C: Solid State Phys.* **1977**, *10*, 2601.
- Atkins, R.; Disch, S.; Jones, Z.; Haeusler, I.; Grosse, C.; Fischer, S. F.; Neumann, W.; Zschack, P.; Johnson, D. C. *J. Solid State Chem.* **2013**, *202*, 128–133.
- Li, F.; Tu, K.; Chen, Z. *J. Phys. Chem. C* **2014**, *118*, 21264–21274.

- (18) Zhao, W.; Dong, B.; Guo, Z.; Su, G.; Gao, R.; Wang, W.; Cao, L. *Chem. Commun.* **2016**, 52, 9228–9231.
- (19) Morales-Guio, C. G.; Stern, L. A.; Hu, X. *Chem. Soc. Rev.* **2014**, 43, 6555–69.
- (20) Braga, D.; Gutiérrez Lezama, I.; Berger, H.; Morpurgo, A. F. *Nano Lett.* **2012**, 12, 5218–5223.
- (21) Zhang, Y. J.; Ye, J. T.; Yomogida, Y.; Takenobu, T.; Iwasa, Y. *Nano Lett.* **2013**, 13, 3023–8.
- (22) Shaik, S.; Mandal, D.; Ramanan, R. *Nat. Chem.* **2016**, 8, 1091–1098.
- (23) Chen, L. D.; Urushihara, M.; Chan, K.; Nørskov, J. K. *ACS Catal.* **2016**, 6, 7133–7139.
- (24) Novoselov, K. S.; Geim, A. K.; Morozov, S. V.; Jiang, D.; Zhang, Y.; Dubonos, S. V.; Grigorieva, I. V.; Firsov, A. A. *Science* **2004**, 306, 666–669.
- (25) Pentland, N.; Bockris, J. M.; Sheldon, E. J. *Electrochem. Soc.* **1957**, 104, 182–194.
- (26) Azizi, O.; Jafarian, M.; Gobal, F.; Heli, H.; Mahjani, M. G. *Int. J. Hydrogen Energy* **2007**, 32, 1755–1761.
- (27) Conway, B.; Tilak, B. *Electrochim. Acta* **2002**, 47, 3571–3594.
- (28) Bockris, J. O. M.; Potter, E. C. J. *Electrochem. Soc.* **1952**, 99, 169–186.
- (29) Thomas, J. G. N. *Trans. Faraday Soc.* **1961**, 57, 1603–1611.
- (30) Perera, M. M.; Lin, M.-W.; Chuang, H.-J.; Chamlagain, B. P.; Wang, C.; Tan, X.; Cheng, M. M.-C.; Tománek, D.; Zhou, Z. *ACS Nano* **2013**, 7, 4449–4458.
- (31) Chen, L.; Lasia, A. J. *Electrochem. Soc.* **1991**, 138, 3321–3328.
- (32) Chuang, H. J.; Chamlagain, B.; Koehler, M.; Perera, M. M.; Yan, J.; Mandrus, D.; Tomanek, D.; Zhou, Z. *Nano Lett.* **2016**, 16, 1896–902.
- (33) Wang, J.; Yan, M.; Zhao, K.; Liao, X.; Wang, P.; Pan, X.; Yang, W.; Mai, L. *Adv. Mater.* **2016**, 29, 1604464.
- (34) Chen, Z.; Cummins, D.; Reinecke, B. N.; Clark, E.; Sunkara, M. K.; Jaramillo, T. F. *Nano Lett.* **2011**, 11, 4168–75.
- (35) Kibsgaard, J.; Chen, Z.; Reinecke, B. N.; Jaramillo, T. F. *Nat. Mater.* **2012**, 11, 963–969.
- (36) Liao, L.; Zhu, J.; Bian, X.; Zhu, L.; Scanlon, M. D.; Girault, H. H.; Liu, B. *Adv. Funct. Mater.* **2013**, 23, 5326–5333.
- (37) Kibsgaard, J.; Jaramillo, T. F.; Besenbacher, F. *Nat. Chem.* **2014**, 6, 248–53.
- (38) Huang, Q.-A.; Park, S.-M. *J. Phys. Chem. C* **2012**, 116, 16939–16950.
- (39) Armstrong, R. D.; Firman, R. E.; Thirsk, H. R. *Faraday Discuss. Chem. Soc.* **1973**, 56, 244–263.
- (40) Armstrong, R. D.; Henderson, M. J. *Electroanal. Chem. Interfacial Electrochem.* **1972**, 39, 81–90.
- (41) Harrington, D. A.; Conway, B. E. *Electrochim. Acta* **1987**, 32, 1703–1712.
- (42) Cummins, D. R.; Martinez, U.; Sherehiy, A.; Kappera, R.; Martinez-Garcia, A.; Schulze, R. K.; Jasinski, J.; Zhang, J.; Gupta, R. K.; Lou, J.; Chhowalla, M.; Sumanasekera, G.; Mohite, A. D.; Sunkara, M. K.; Gupta, G. *Nat. Commun.* **2016**, 7, 11857.
- (43) Grahame, D. C. *Chem. Rev.* **1947**, 41, 441–501.
- (44) Ding, M.; He, Q.; Wang, G.; Cheng, H. C.; Huang, Y.; Duan, X. *Nat. Commun.* **2015**, 6, 7867.
- (45) Conway, B.; Gileadi, E. *Trans. Faraday Soc.* **1962**, 58, 2493–2509.
- (46) Barbieri, O.; Hahn, M.; Herzog, A.; Kötz, R. *Carbon* **2005**, 43, 1303–1310.
- (47) Mysyk, R.; Raymundo-Piñero, E.; Béguin, F. *Electrochem. Commun.* **2009**, 11, 554–556.
- (48) Zheng, J. P. *J. Electrochem. Soc.* **1997**, 144, 2026–2031.
- (49) Pell, W. G.; Conway, B. E.; Marincic, N. *J. Electroanal. Chem.* **2000**, 491, 9–21.
- (50) Gupta, N.; Gattrell, M.; MacDougall, B. J. *Appl. Electrochem.* **2006**, 36, 161–172.
- (51) Liu, M.; Pang, Y.; Zhang, B.; De Luna, P.; Voznyy, O.; Xu, J.; Zheng, X.; Dinh, C. T.; Fan, F.; Cao, C.; de Arquer, F. P.; Safaei, T. S.; Mepham, A.; Klinkova, A.; Kumacheva, E.; Filleter, T.; Sinton, D.; Kelley, S. O.; Sargent, E. H. *Nature* **2016**, 537, 382–386.